

Exotic synchronization in continuous time crystals outside the symmetric subspace

Parvinder Solanki,^{1,*} Midhun Krishna,² Michal Hajdušek,^{3,4,†} Christoph Bruder,¹ and Sai Vinjanampathy^{2,5,6,‡}

¹*Department of Physics, University of Basel, Klingelbergstrasse 82, CH-4056 Basel, Switzerland*

²*Department of Physics, Indian Institute of Technology-Bombay, Powai, Mumbai 400076, India*

³*Keio University Shonan Fujisawa Campus, 5322 Endo, Fujisawa, Kanagawa 252-0882, Japan*

⁴*Keio University Quantum Computing Center, 3-14-1 Hiyoshi, Kohoku, Yokohama, Kanagawa 223-8522, Japan*

⁵*Centre of Excellence in Quantum Information, Computation, Science and Technology,*

Indian Institute of Technology Bombay, Powai, Mumbai 400076, India

⁶*Centre for Quantum Technologies, National University of Singapore, 3 Science Drive 2, Singapore 117543*

(Dated: January 2, 2024)

Exploring continuous time crystals (CTCs) within the symmetric subspace of spin systems has been a subject of intensive research in recent times. Thus far, the stability of the time-crystal phase outside the symmetric subspace in such spin systems has gone largely unexplored. Here, we investigate the effect of including the asymmetric subspaces on the dynamics of CTCs in a driven dissipative spin model. This results in multistability, and the dynamics becomes dependent on the initial state. Remarkably, this multistability leads to exotic synchronization regimes such as chimera states and cluster synchronization in an ensemble of coupled identical CTCs.

Introduction.— Crystals have traditionally been characterized by their spatial periodicity, wherein atoms are arranged in a repeating pattern. Time crystals showcase a distinct form of periodicity, namely in the temporal dimension [1–4]. Initially, time crystals breaking discrete time-translation symmetry were conceptualized and termed discrete time crystals [3–12]. A more recent development in the field has been the emergence of continuous time crystals (CTCs) [13–29], which break continuous time-translation symmetry. CTCs were initially discussed in the context of a driven dissipative Dicke model [13]. Their behavior was also studied in other spin systems like collective d -level systems [21], p - q interacting spin models [22], spin star models [25], and spin systems with infinite-range interactions [27]. In addition to the time-crystal behavior, the thermodynamics [30] of driven Dicke models and the occurrence of entanglement phase transitions [31, 32] have also been investigated recently. The application of time-crystal phases in sensing [33, 34] and quantum engines [35] has been proposed. Furthermore, experimental platforms such as Bose-Einstein condensate systems have been used to realize CTCs [36, 37].

All of these examples are variants of the Dicke model: the system is a collective spin that is built up of N spins $1/2$. These systems are characterized by permutational symmetry which is a strong symmetry of the underlying open quantum system [38, 39]. Previous investigations of both superradiance [40–43] and time-crystal behavior have focused on the totally symmetric Dicke subspace, which corresponds to the maximum-excitation subspace. The assumption of permutational symmetry is not always straightforward to enforce under realistic conditions [44]. This leads to the important open question of the role played by the lower-excitation subspaces involving asymmetric Dicke states in the dynamics of time crystals. Recent studies have shown that asymmetric subspaces are crucial for understanding subradiant phases [45–48] and

the thermodynamics of permutation-invariant quantum many-body systems [49–51].

In this Letter, we investigate the existence of time crystals outside the symmetric Dicke subspace in a spin-only description of the driven dissipative Dicke model [13, 24]. We show that incorporating the asymmetric subspaces enhances the complexity and richness of CTC dynamics and yields an extended phase diagram. Using mean-field analysis, we find that CTCs exhibit multistability in the asymmetric subspaces, which was not observed for CTCs restricted to the symmetric subspace. The existence of multistability is confirmed by analyzing the eigenspectra of the Liouville superoperator that describes the Markovian dynamics of open quantum systems [38, 52, 53]. Depending on the system parameters, an initial state outside the symmetric subspace can always be found which breaks time-translational symmetry. Interestingly, this initial-state dependence leads to exotic synchronization phenomena like chimera states in a network of coupled identical CTCs that are characterized by the coexistence of synchronized and unsynchronized regions [54, 55]. Furthermore, such a network of CTCs also exhibits cluster synchronization, where identical oscillators arrange themselves into two or more differently synchronized clusters [56].

We begin with an investigation of the mean-field dynamics of a collective spin using fixed-point analysis, which describes the steady-state dynamics of the system. Then, we will use Liouville superoperator theory to validate the mean-field results. Finally, we discuss the existence of a chimera state and cluster synchronization in coupled CTCs before summarizing our results.

Mean-field analysis and phase diagram.— The master equation governing the dynamics of the CTC [13, 24]

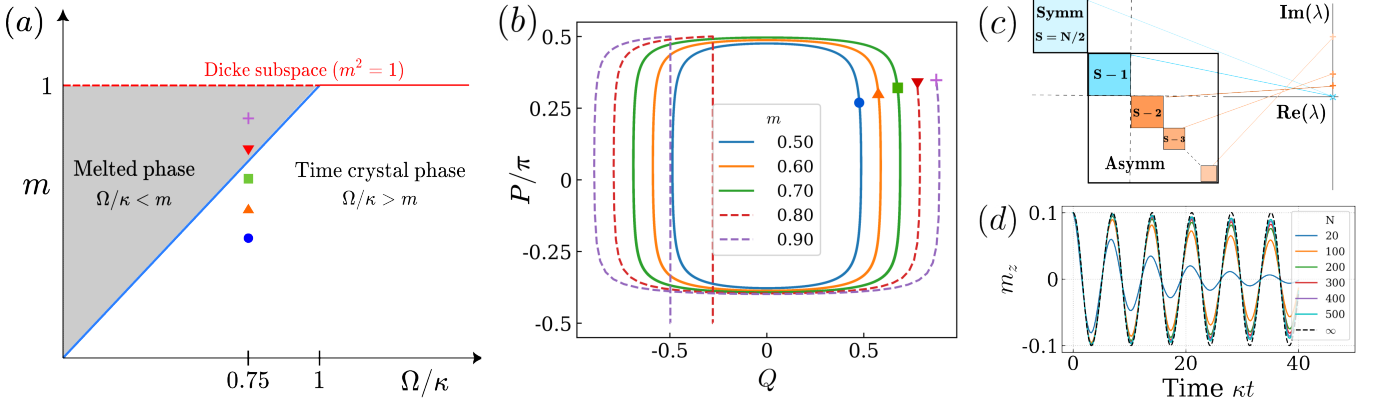


FIG. 1. (a) Phase diagram of a continuous time crystal (CTC) characterized using fixed-point analysis of mean-field equations with $m = \langle \hat{S} \rangle / S$. (b) Phase-space portrait of the CTC for various initial states (indicated by different symbols in (a)) for $\Omega/\kappa = 0.75$. (c) Schematic representation of block diagonal structure of Liouville superoperator $\mathcal{L} = \mathcal{L}_S + \mathcal{L}_A$ where $\mathcal{L}_{S(A)}$ corresponds to symmetric (asymmetric) Dicke subspace. Here, dotted lines separate the blocks with $m > \Omega/\kappa$ from those with $m < \Omega/\kappa$. Only the sub-blocks having rescaled magnetization value $m < \Omega/\kappa$ will have purely imaginary eigenvalues in the thermodynamic limit $S \rightarrow \infty$. (d) Oscillations of m_z for an initial state prepared in the asymmetric subspace $m = 0.1$ for $\Omega/\kappa = 0.9$.

is given by

$$\dot{\rho} = \mathcal{L}_{\Omega, \kappa}(\rho) = -i[\Omega \hat{S}_x, \rho] + \frac{\kappa}{S}(\hat{S}_- \rho \hat{S}_+ - \frac{1}{2}\{\hat{S}_+ \hat{S}_-, \rho\}), \quad (1)$$

where $\mathcal{L}_{\Omega, \kappa}$ is the Liouville superoperator, $\hat{S}_\alpha = \sum_i \sigma_\alpha^i / 2$ are collective spin operators where $\alpha \in \{x, y, z\}$, $S = N/2$ is the maximum spin value for N spins $1/2$ and $\hat{S}_\pm = \hat{S}_x \pm i\hat{S}_y$. The dynamics of the given system in the thermodynamic limit ($N \rightarrow \infty$) can be well understood using mean-field analysis. The evolution of mean-field expectation values of the rescaled spin operators, $m_\alpha = \langle \hat{S}_\alpha \rangle / S$ is governed by

$$\begin{aligned} \dot{m}_x &= \kappa m_x m_z, \\ \dot{m}_y &= -\Omega m_z + \kappa m_y m_z, \\ \dot{m}_z &= \Omega m_y - \kappa [m_x^2 + m_y^2]. \end{aligned} \quad (2)$$

The total spin of the system is conserved since \hat{S}^2 commutes with all other spin operators in Eq. (1) and hence is a strong symmetry of the system [38, 52, 57]. At the mean-field level, this implies that $m_x^2 + m_y^2 + m_z^2 = m^2$ is a conserved quantity since correlations are assumed to vanish. For the symmetric Dicke subspace, m is constrained to take the value 1, which led to the breaking of time-translational symmetry at $\Omega/\kappa = 1$ in earlier studies [13, 24].

We will now consider the more general case $0 \leq m < 1$. The fixed points, (m_x^*, m_y^*, m_z^*) , of the coupled differential Eqs. (2) for this case are given as $\mathcal{M}_1 = (\pm m \sqrt{1 - (m\kappa/\Omega)^2}, m^2 \kappa / \Omega, 0)$ and $\mathcal{M}_2 = (0, \Omega/\kappa, \pm \sqrt{m^2 - (\Omega/\kappa)^2})$. The stability of these fixed points is given by the eigenvalues of the Jacobian \mathcal{J} , whose matrix elements are defined as $\mathcal{J}_{\alpha\beta} = dm_\alpha / dm_\beta$.

The eigenvalues of \mathcal{J} corresponding to fixed points \mathcal{M}_1 and \mathcal{M}_2 are $\{\Lambda_1\} = \{0, \pm \kappa \sqrt{m^2 - (\Omega/\kappa)^2}\}$ and $\{\Lambda_2\} = \{0, \pm \kappa \sqrt{m^2 - (\Omega/\kappa)^2}, \pm \kappa \sqrt{m^2 - (\Omega/\kappa)^2}\}$ respectively, where both the upper or both the lower signs have to be chosen together. Note that the dynamics of the system are now dependent on both the system parameters Ω/κ and rescaled total magnetization m of the given spin-subspace. For $\Omega/\kappa < m$, \mathcal{M}_2 is the only physical state of the system since \mathcal{M}_1 has unphysical imaginary values for the expectation of spin components. The corresponding eigenvalues $\{\Lambda_2\}$ for the fixed point \mathcal{M}_2 are purely real, and hence it is a saddle fixed point of the system. Therefore, the system relaxes to a time-invariant state given by the fixed point \mathcal{M}_2 for initial states having $m > \Omega/\kappa$, and no time-crystal behavior is observed. For states with $m < \Omega/\kappa$, \mathcal{M}_1 is the only physical fixed point of the system. The eigenvalues $\{\Lambda_1\}$ for the fixed point \mathcal{M}_1 are purely imaginary, and hence, the corresponding fixed point is a center. Therefore, the system oscillates in time for initial states having $m < \Omega/\kappa$, and time-translational symmetry is broken even for $\Omega/\kappa < 1$.

Using this fixed-point analysis, we can characterize the phase transition of the system as described by Fig. 1(a). The system exhibits multistability for $\Omega/\kappa < 1$. The two fixed points \mathcal{M}_1 and \mathcal{M}_2 have different basins of attraction: depending upon the initial state, the system can exhibit two different phases, namely, a melted and a time-crystal phase. For the Dicke subspace, this bistability does not exist, as depicted in Fig. 1(a). The Dicke subspace corresponds to initial states having $m = 1$, which shows that for $\Omega/\kappa < 1$, the system always settles down to a saddle fixed point (dashed red line), and for $\Omega/\kappa > 1$, it shows oscillatory behavior (solid red line). However, for $m < 1$, both time-translation invariant and

symmetry-broken phases coexist and are separated by the blue line corresponding to $m = \Omega/\kappa$. Initial states having $m > \Omega/\kappa$ on the left of $m = \Omega/\kappa$ (blue) line settle down to the saddle fixed point \mathcal{M}_2 . The parameter region right to the $m = \Omega/\kappa$ (blue) line corresponds to $m < \Omega/\kappa$ and gives stable oscillations around the fixed point \mathcal{M}_1 leading to time-translational symmetry breaking.

To illustrate the phase-space portrait of the fixed points discussed above, we consider the following coordinate transformation $P = \tan^{-1}[m_y/m_x]$, $Q = m_z$ [13]. In terms of the new co-ordinates P and Q , the fixed points $\{P^*, Q^*\}$ are given as $\mathcal{M}_1^{P,Q} = (\tan^{-1}[\pm 1/\sqrt{(\Omega/m\kappa)^2 - 1}], 0)$ and $\mathcal{M}_2^{P,Q} = (\pm\pi/2, \pm\sqrt{m^2 - (\Omega/\kappa)^2})$. The phase-space portrait of the CTC for different m values is depicted in Fig. 1(b) for $\Omega/\kappa = 0.75$. Initial states having $m < \Omega/\kappa$ keep oscillating in the vicinity of the fixed point $\mathcal{M}_1^{P,Q}$. As soon as we choose an initial state with $m > \Omega/\kappa$, the corresponding trajectory in Fig. 1(b) settles down to the saddle fixed point $\mathcal{M}_2^{P,Q}$. For $\Omega/\kappa > 1$, there exists no physical state of the system that can have $m > \Omega/\kappa$ since $m \leq 1$ for the rescaled spin operators. The stability of the oscillations around the fixed point $\mathcal{M}_1^{P,Q}$ can be verified by observing Fig. 1(b), where each limit cycle trajectory consists of around 4000 cycles of oscillations. These trajectories are obtained by the time evolution of the exact mean-field equations (2) (including non-linear terms) and show no deviation even at such long times.

Role of asymmetric subspaces.— We now go beyond mean-field theory and study the full master equation Eq. (1). The Hilbert space of the ensemble consisting of N spins can be described as a direct sum of irreducible representations of $SU(2)$ using the Clebsch-Gordan decomposition [58]. Since \hat{S}^2 is a strong symmetry of the dynamics, the Liouville superoperator block-diagonalizes [38, 59] in respective spin- J eigenbases such that $\mathcal{L} = \oplus \mathcal{L}_J$, as shown in Fig. 1(c). Therefore, the dynamics is constrained within each spin- J subspace (invariant subspaces of dynamics). The maximum angular momentum value $J = S = N/2$ corresponds to the totally symmetric Dicke subspace; lower J values correspond to asymmetric subspaces. The spin- J irreducible representation has dimension $2J + 1$ and multiplicity $n_J = N!(2J + 1)/(N/2 + J + 1)!(N/2 - J)!$ [51, 60, 61]. The total Hilbert space is spanned by the generalized Dicke basis, $\{|J, m_J, \mu_J\rangle\}$. Here, $J \in \{S, S - 1 \dots J_0\}$, $m_J \in \{J, J - 1 \dots -(J - 1), -J\}$ and $1 \leq \mu_J \leq n_J$, with $J_0 = 0$ or 1 depending on whether N is even or odd. We can associate each of the spin- J subspaces with the mean-field total angular momentum value $m = J/S$. The states with $m < 1$ belong to the asymmetric angular momentum sectors.

The mean-field analysis suggests that for any given value of Ω/κ , we can always find an initial state hav-

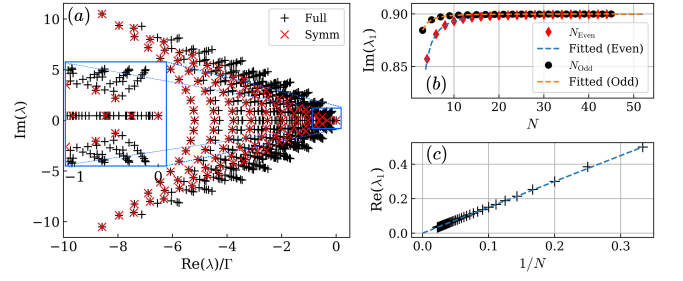


FIG. 2. (a) Eigenspectra of $\mathcal{L}_{\Omega, \kappa}$ for symmetric and full Hilbert space (indicated by ‘ \times ’ and ‘+’, respectively) with $\Omega/\kappa = 0.9$ (same for all subfigures) and $N = 10$. (b) The imaginary part of the first dominant eigenvalue λ_1 tends to 0.9 (i.e., the value of Ω) in the thermodynamic limit and is consistent with mean-field analysis. (c) The real part of λ_1 scales as $1/N$ and tends to zero in the thermodynamic limit. All the eigenvalues shown here are in units of κ .

ing $m < \Omega/\kappa$ such that the system oscillates in time. In terms of parameters rescaled by m , the critical point is located at $\Omega/(m\kappa) = 1$ for each invariant subspace. The well-studied case with $J = S$ describing the symmetric subspace (with dimension $N + 1$) has $m = 1$ and a critical point at $\Omega/\kappa = 1$. The remainder of the Hilbert space with dimension $2^N - (N + 1)$ spans the asymmetric subspaces and has $m < 1$. Hence, even for $\Omega/\kappa < 1$, the exact dynamics of the finite-size system exhibits time-crystal behavior. Figure 1(d) depicts the time evolution with the initial state belonging to the $m = 0.1$ subspace, having $\{m_x, m_y, m_z\} = \{0, 0, 0.1\}$ for $\Omega/\kappa = 0.9$. As the system size increases, the oscillation in m_z becomes persistent and approaches the mean-field limit. Any initial state belonging to the $m > 0.9$ subspace will decay and go to a time-invariant steady state irrespective of system size. Thus, the exact treatment confirms the mean-field analysis for $\Omega/\kappa < 1$.

The time-crystal phase is characterized by the spectral gap closing of the Liouvillian eigenspectra in the thermodynamic limit, with the leading eigenvalue being purely imaginary. For the symmetric subspace, the spectral gap of \mathcal{L}_S closes only for $\Omega/\kappa > 1$. Including the asymmetric subspaces $\mathcal{L}_A = \oplus_{J < S} \mathcal{L}_J$ introduces new leading-order eigenvalues, as shown in Fig. 2(a). Therefore, the spectral gap closes even for $\Omega/\kappa < 1$, as depicted in Figs. 2(b)–(c). The first dominant eigenvalue in the asymmetric subspace scales differently for even and odd N , but converges to the same value for large values of N , as shown in Fig. 2(b). The real part of the eigenvalue λ_1 for both even and odd values of N scales as $1/N$ with the same slope as shown in Fig. 2(c) and vanishes in the thermodynamic limit. This means that the spectral gap closes even for $\Omega/\kappa < 1$ for the asymmetric subspaces. Therefore, time crystal behavior can be observed outside the permutational symmetric subspace even for $\Omega/\kappa < 1$ if the initial state belongs to an asymmetric subspace

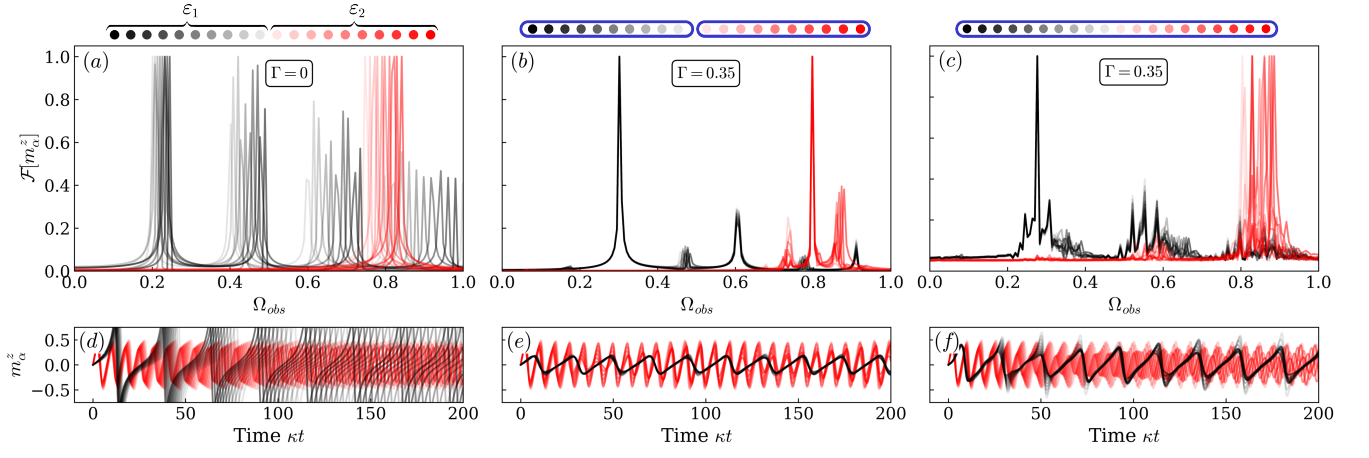


FIG. 3. Normalized Fourier transform $\mathcal{F}[m_\alpha^z]$ (a-c) and time evolution of m_α^z (d-f) for $n = 20$ continuous time crystals (CTCs). All the CTCs are identical ($\Omega_\alpha/\kappa = 0.9$ and $\kappa = 1$) and are initialized in different m subspaces. The two ensembles $\varepsilon_{1,2}$ are represented by the colors black and red above subfigures (a,b,c), and the CTCs within one ensemble by different intensities. Subfigures (a,d) show the case of uncoupled time crystals. Coupling CTCs within each ensemble with a coupling strength of $\Gamma/\kappa = 0.35$ results in the synchronization of CTCs within the ensemble as shown in (b,e). In subfigures (c,f) all CTCs are coupled. Surprisingly, CTCs in ensemble ε_1 get synchronized, while the CTCs in the ensemble ε_2 remain unsynchronized: the system exhibits a *chimera* state.

having $m < \Omega/\kappa$.

Chimera state in coupled CTCs.— We now discuss the effect of including asymmetric subspaces on the dynamics of n coherently coupled CTCs described by the following master equation,

$$\dot{\rho} = \sum_{\alpha} \mathcal{L}_{\Omega_{\alpha}, \kappa_{\alpha}}(\rho) - \frac{i}{n} \left[\sum_{\beta \neq \alpha} \Gamma_{\alpha, \beta} (\hat{S}_+^{\alpha} \hat{S}_-^{\beta} + \hat{S}_-^{\alpha} \hat{S}_+^{\beta}), \rho \right]. \quad (3)$$

Here, $\mathcal{L}_{\Omega_{\alpha}, \kappa_{\alpha}}(\rho)$ describes the dynamics of uncoupled CTCs, and $\Gamma_{\alpha, \beta}$ is the coupling strength between two CTCs α and β . Such an interaction resulted in the observation of the seeding effect and the synchronization of detuned CTCs considering only the symmetric subspace [24]. We now also take into account asymmetric subspaces and assume that all the CTCs are identical, $\mathcal{L}_{\Omega_{\alpha}, \kappa_{\alpha}} = \mathcal{L}_{\Omega, \kappa}$, $\forall \alpha$. Even if they are identical, different choices of initial states can lead to surprising disparate effects in the dynamics. We investigate the mean-field dynamics of $n = 20$ coupled CTCs in Fig. 3, where all CTCs are initialized in asymmetric subspaces belonging to different values of m . The corresponding frequency and the dynamics of m_z^{α} of uncoupled CTCs depending on the value m are shown in Fig. 3(a) and Fig. 3(d), respectively. Depending on the frequency distribution given by Fig. 3(a), the system splits into two ensembles ε_1 and ε_2 which are indicated by black and red colors, respectively. First, we consider the case where CTCs within the same ensemble are coupled with a finite interaction strength but there is no coupling between CTCs of different ensembles such that $\Gamma_{\alpha, \beta} = \Gamma \delta_{\varepsilon_i \varepsilon_j} \forall (\alpha \in \varepsilon_i, \beta \in \varepsilon_j)$. This results in the synchronization of CTCs within the same ensemble as shown by Fig. 3(b,e). Surprisingly,

considering all-to-all coupled CTCs ($\Gamma_{\alpha, \beta}/\kappa = \Gamma/\kappa = 0.35 \forall (\alpha, \beta)$) leads to the synchronization of the CTCs only in one ensemble (here ε_1), while the CTCs in the other ensemble (here ε_2) exhibit unsynchronized dynamics as shown in Fig. 3(c,f). Such surprising patterns of partial synchronization in systems of coupled identical non-linear oscillators were first observed in [54] and were called *chimera states* [55, 62]. First strides towards chimera states in quantum systems involved exploring one-dimensional arrays of quantum oscillators [63] and periodically driven networks of spins [12]. Our work demonstrates a chimera state in a system of coupled identical CTCs. Here, the chimera state results from including the asymmetric subspaces into the dynamics of identical CTCs, allowing us to choose an initial state with different frequencies in different subspaces [64]. Increasing the coupling strength results in the synchronization of all CTCs (see Appendix B). Another example of an exotic synchronization regime that can be realized in coupled identical CTCs is *cluster synchronization* where the system separates into two differently synchronized clusters. Note that such complex dynamics can be obtained for arbitrary initial conditions (see Appendix C).

Conclusions.— In this work, we focused on the fundamental question of whether continuous time crystals in spin models only exist if initialized in the symmetric subspace. Our first main result is that the inclusion of asymmetric subspaces leads to time-crystal behavior even if the ratio of drive to dissipation strength Ω/κ is less than one. A second result is that taking into account asymmetric subspaces leads to multistability: depending on the parameter values, the system can exhibit a time crystal or melted phase for different initial states. For an

ensemble of coupled CTCs, this leads to our third result, the existence of chimera states and cluster synchronization, which is not possible for CTCs realized in the symmetric subspace. Our results provide new insights into the dynamics of time-crystal phases and point out strategies in the design of quantum networks that may lead to the observation of exotic synchronization phenomena.

An interesting future direction is to study the effect of weak permutational symmetry-breaking interactions, which allow the system to move between various spin sectors. Such interactions are inevitable in various experimental settings and will offer further valuable insights into the fundamental characteristics of time crystals.

Acknowledgments. — P.S. and S.V. thank R. Fazio for discussions. Numerical calculations were performed using QuTiP [65, 66] and PIQS [67]. M.H. was supported by [MEXT Quantum Leap Flagship Program] Grants No. JPMXS0118067285 and No. JPMXS0120319794. P.S. and C.B. acknowledge financial support from the Swiss National Science Foundation individual grant (grant no. 200020_200481). S.V. acknowledges support from DST-QUEST grant number DST/ICPS/QuST/Theme-4/2019. While preparing the manuscript, we became aware of related work [68].

* parvinder.parvinder@unibas.ch

† michal@sfc.wide.ad.jp

‡ sai@phy.iitb.ac.in

- [1] F. Wilczek, *Phys. Rev. Lett.* **109**, 160401 (2012).
- [2] H. Watanabe and M. Oshikawa, *Phys. Rev. Lett.* **114**, 251603 (2015).
- [3] M. P. Zaletel, M. Lukin, C. Monroe, C. Nayak, F. Wilczek, and N. Y. Yao, *Rev. Mod. Phys.* **95**, 031001 (2023).
- [4] K. Sacha and J. Zakrzewski, *Reports on Progress in Physics* **81**, 016401 (2017).
- [5] K. Sacha, *Phys. Rev. A* **91**, 033617 (2015).
- [6] D. V. Else, B. Bauer, and C. Nayak, *Phys. Rev. Lett.* **117**, 090402 (2016).
- [7] V. Khemani, A. Lazarides, R. Moessner, and S. L. Sondhi, *Phys. Rev. Lett.* **116**, 250401 (2016).
- [8] A. Russomanno, F. Iemini, M. Dalmonte, and R. Fazio, *Phys. Rev. B* **95**, 214307 (2017).
- [9] F. M. Surace, A. Russomanno, M. Dalmonte, A. Silva, R. Fazio, and F. Iemini, *Phys. Rev. B* **99**, 104303 (2019).
- [10] T. L. Heugel, M. Oscity, A. Eichler, O. Zilberberg, and R. Chitra, *Phys. Rev. Lett.* **123**, 124301 (2019).
- [11] R. Khasseh, R. Fazio, S. Ruffo, and A. Russomanno, *Phys. Rev. Lett.* **123**, 184301 (2019).
- [12] A. Sakurai, V. M. Bastidas, W. J. Munro, and K. Nemoto, *Phys. Rev. Lett.* **126**, 120606 (2021).
- [13] F. Iemini, A. Russomanno, J. Keeling, M. Schirò, M. Dalmonte, and R. Fazio, *Phys. Rev. Lett.* **121**, 035301 (2018).
- [14] K. Tucker, B. Zhu, R. J. Lewis-Swan, J. Marino, F. Jimenez, J. G. Restrepo, and A. M. Rey, *New Journal of Physics* **20**, 123003 (2018).
- [15] B. Buča, J. Tindall, and D. Jaksch, *Nature Communications* **10**, 1 (2019).
- [16] C. Booker, B. Buča, and D. Jaksch, *New Journal of Physics* **22**, 085007 (2020).
- [17] B. Buča and D. Jaksch, *Phys. Rev. Lett.* **123**, 260401 (2019).
- [18] B. Zhu, J. Marino, N. Y. Yao, M. D. Lukin, and E. A. Demler, *New Journal of Physics* **21**, 073028 (2019).
- [19] C. Lledó, T. K. Mavrogordatos, and M. H. Szymańska, *Phys. Rev. B* **100**, 054303 (2019).
- [20] K. Seibold, R. Rota, and V. Savona, *Phys. Rev. A* **101**, 033839 (2020).
- [21] L. F. d. Prazeres, L. d. S. Souza, and F. Iemini, *Phys. Rev. B* **103**, 184308 (2021).
- [22] G. Piccitto, M. Wauters, F. Nori, and N. Shammah, *Phys. Rev. B* **104**, 014307 (2021).
- [23] F. Carollo and I. Lesanovsky, *Phys. Rev. A* **105**, L040202 (2022).
- [24] M. Hajdušek, P. Solanki, R. Fazio, and S. Vinjanampathy, *Phys. Rev. Lett.* **128**, 080603 (2022).
- [25] M. Krishna, P. Solanki, M. Hajdušek, and S. Vinjanampathy, *Phys. Rev. Lett.* **130**, 150401 (2023).
- [26] R. Hurtado-Gutiérrez, F. Carollo, C. Pérez-Espigares, and P. I. Hurtado, *Phys. Rev. Lett.* **125**, 160601 (2020).
- [27] J. G. Cosme, J. Skulte, and L. Mathey, *Phys. Rev. B* **108**, 024302 (2023).
- [28] G. Buonaiuto, F. Carollo, B. Olmos, and I. Lesanovsky, *Phys. Rev. Lett.* **127**, 133601 (2021).
- [29] A. Cabot, G. Giorgi, and R. Zambrini, (2023), [arXiv:2308.12080 \[quant-ph\]](https://arxiv.org/abs/2308.12080).
- [30] F. Carollo, I. Lesanovsky, M. Antezza, and G. De Chiara, (2023), [arXiv:2306.07330 \[quant-ph\]](https://arxiv.org/abs/2306.07330).
- [31] G. Passarelli, P. Lucignano, R. Fazio, and A. Russomanno, *Phys. Rev. B* **106**, 224308 (2022).
- [32] A. Cabot, L. S. Muhle, F. Carollo, and I. Lesanovsky, *Phys. Rev. A* **108**, L041303 (2023).
- [33] A. Cabot, F. Carollo, and I. Lesanovsky, (2023), [arXiv:2307.13277 \[quant-ph\]](https://arxiv.org/abs/2307.13277).
- [34] V. Montenegro, M. G. Genoni, A. Bayat, and M. G. Paris, *Communications Physics* **6**, 304 (2023).
- [35] F. Carollo, K. Brandner, and I. Lesanovsky, *Phys. Rev. Lett.* **125**, 240602 (2020).
- [36] H. Keßler, P. Kongkhambut, C. Georges, L. Mathey, J. G. Cosme, and A. Hemmerich, *Phys. Rev. Lett.* **127**, 043602 (2021).
- [37] P. Kongkhambut, J. Skulte, L. Mathey, J. G. Cosme, A. Hemmerich, and H. Keßler, *Science* **377**, 670 (2022).
- [38] B. Buča and T. Prosen, *New Journal of Physics* **14**, 073007 (2012).
- [39] V. V. Albert and L. Jiang, *Phys. Rev. A* **89**, 022118 (2014).
- [40] R. H. Dicke, *Phys. Rev.* **93**, 99 (1954).
- [41] A. V. Andreev, V. I. Emel'yanov, and Y. A. Il'inskiĭ, *Soviet Physics Uspekhi* **23**, 493 (1980).
- [42] Y. K. Wang and F. Hioe, *Phys. Rev. A* **7**, 831 (1973).
- [43] M. O. Scully and A. A. Svidzinsky, *Science* **325**, 1510 (2009).
- [44] G. Ferioli, A. Glicenstein, I. Ferrier-Barbut, and A. Browaeys, *Nature Physics* **19**, 1345 (2023).
- [45] D. Bhatti, R. Schneider, S. Oppel, and J. von Zanthier, *Phys. Rev. Lett.* **120**, 113603 (2018).
- [46] M. Bojer and J. von Zanthier, *Phys. Rev. A* **106**, 053712 (2022).
- [47] M. Gegg, A. Carmele, A. Knorr, and M. Richter, *New*

- Journal of Physics* **20**, 013006 (2018).
- [48] R. Wiegner, J. von Zanthier, and G. S. Agarwal, *Phys. Rev. A* **84**, 023805 (2011).
- [49] C. L. Latune, I. Sinayskiy, and F. Petruccione, *Phys. Rev. Res.* **1**, 033192 (2019).
- [50] C. L. Latune, I. Sinayskiy, and F. Petruccione, *New Journal of Physics* **22**, 083049 (2020).
- [51] B. Yadin, B. Morris, and K. Brandner, *Phys. Rev. Res.* **5**, 033018 (2023).
- [52] V. V. Albert and L. Jiang, *Phys. Rev. A* **89**, 022118 (2014).
- [53] M. Krishna, P. Solanki, and S. Vinjanampathy, *Journal of the Indian Institute of Science* **103**, 513 (2023).
- [54] Y. Kuramoto and D. Battogtokh, *Nonlinear Phenom. Complex Syst.* **5**, 380 (2002).
- [55] D. M. Abrams and S. H. Strogatz, *Phys. Rev. Lett.* **93**, 174102 (2004).
- [56] S. W. Haugland, *Journal of Physics: Complexity* **2**, 032001 (2021).
- [57] D. Manzano and P. Hurtado, *Advances in Physics* **67**, 1 (2018).
- [58] J. J. Sakurai and E. D. Commins, *Modern quantum mechanics, revised edition* (American Association of Physics Teachers, 1995).
- [59] J. Thingna and D. Manzano, *Chaos: An Interdisciplinary Journal of Nonlinear Science* **31**, 073114 (2021).
- [60] H. Georgi, *Lie algebras in particle physics: from isospin to unified theories* (Taylor & Francis, 2000).
- [61] P. Ramadevi and V. Dubey, *Group Theory for Physicists: With Applications* (Cambridge University Press, 2019).
- [62] A. Zakharova, *Chimera patterns in networks* (Springer, 2020).
- [63] V. M. Bastidas, I. Omelchenko, A. Zakharova, E. Schöll, and T. Brandes, *Phys. Rev. E* **92**, 062924 (2015).
- [64] S. R. Ujjwal, N. Punetha, A. Prasad, and R. Ramaswamy, *Phys. Rev. E* **95**, 032203 (2017).
- [65] J. Johansson, P. Nation, and F. Nori, *Computer Physics Communications* **183**, 1760 (2012).
- [66] J. Johansson, P. Nation, and F. Nori, *Computer Physics Communications* **184**, 1234 (2013).
- [67] N. Shammah, S. Ahmed, N. Lambert, S. De Liberato, and F. Nori, *Phys. Rev. A* **98**, 063815 (2018).
- [68] F. Iemini, D. Chang, and J. Marino, (2023), [arXiv:2309.10746](https://arxiv.org/abs/2309.10746) [quant-ph].

Appendix A: Mean-field equations for coupled continuous time crystals

Here we discuss the mean-field dynamics of the coherently coupled CTCs described by Eq. (3) of the main text. These equations are formulated in terms of the rescaled spin operators $m_\alpha = \langle \hat{S}_\alpha \rangle / S$ and are defined as follows,

$$\begin{aligned}
 \frac{d\langle \hat{m}_\alpha^x \rangle}{dt} &= \kappa \langle \hat{m}_\alpha^x \rangle \langle \hat{m}_\alpha^z \rangle + \frac{\Gamma}{n} \langle \hat{m}_\alpha^z \rangle \sum_{\beta \neq \alpha} \langle \hat{m}_\beta^y \rangle, \\
 \frac{d\langle \hat{m}_\alpha^y \rangle}{dt} &= -\Omega_\alpha \langle \hat{m}_\alpha^z \rangle + \kappa \langle \hat{m}_\alpha^y \rangle \langle \hat{m}_\alpha^z \rangle - \frac{\Gamma}{n} \langle \hat{m}_\alpha^z \rangle \sum_{\beta \neq \alpha} \langle \hat{m}_\beta^x \rangle, \\
 \frac{d\langle \hat{m}_\alpha^z \rangle}{dt} &= \Omega_\alpha \langle \hat{m}_\alpha^y \rangle - \kappa [\langle \hat{m}_\alpha^x \rangle^2 + \langle \hat{m}_\alpha^y \rangle^2] + \frac{\Gamma}{n} \left[\langle \hat{m}_\alpha^y \rangle \sum_{\beta \neq \alpha} \langle \hat{m}_\beta^x \rangle - \langle \hat{m}_\alpha^x \rangle \sum_{\beta \neq \alpha} \langle \hat{m}_\beta^y \rangle \right].
 \end{aligned} \tag{4}$$

We numerically solve these coupled differential equations to study the synchronization of coupled CTCs.

Appendix B: Chimera state and synchronization via seeding

The initial state leading to the chimera state shown in Fig. 3 of the main text is chosen such that the absolute value of corresponding eigenvalue $\{|\lambda_1^\alpha|; \alpha = 1 \dots 20\}$ for the fixed point \mathcal{M}_1 has an equal distribution from 0.2 to 0.25 for CTCs in ensemble ε_1 (represented by black color) and from 0.75 to 0.85 for CTCs in ensemble ε_2 (represented by red color). For the given initial state, we investigate the effect of increasing the coupling strength between the all-to-all coupled CTCs on the synchronization properties. For coupling strength $\Gamma/\kappa = 0.5$, all the CTCs in ensemble ε_1 are synchronized while CTCs in ensemble ε_2 only show partial synchronization, as shown in Figs. 4(a,d). Increasing Γ we see more complex dynamics (not shown here), but the system continues to exhibit a chimera state. At $\Gamma/\kappa \approx 0.605$, a transition occurs: the strength of the coupling leads to the melting of the CTCs of ensemble ε_1 as depicted in Figs. 4(b,e). Further increasing the coupling strength leads to the synchronization of the CTCs in ensemble ε_2 which seeds oscillations to ensemble ε_1 . As a result, at coupling strength $\Gamma/\kappa = 1.2$, all the CTCs oscillate with a common frequency as shown in Figs. 4(c,f). Such a synchronization via seeding is consistent with what was observed in [24].

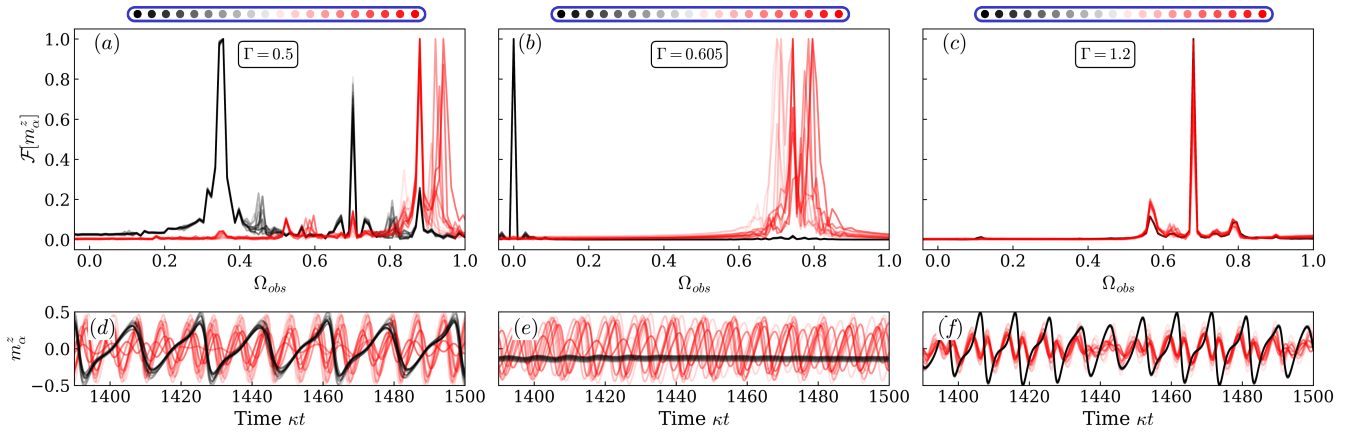


FIG. 4. Normalized Fourier transform $\mathcal{F}[m_\alpha^z]$ (c-d) and time evolution of m_α^z (d-f) for coupling strength $\Gamma/\kappa = 0.5$ (a,d), $\Gamma/\kappa = 0.605$ (b,e) and $\Gamma/\kappa = 1.2$ (c,f).

Appendix C: Cluster synchronization

We will now discuss the effect of small changes in the initial state on the synchronization of CTCs. As an example, we consider a change in the initial states for CTCs belonging to ensemble ε_2 such that the distribution of $\{|\lambda_1^\alpha|\}$ is from 0.75 to 0.8. The choice of initial states for the uncoupled CTCs is shown in Figs. 5(a,d). Now we study the effect of choosing this distribution on the synchronization of CTCs and we only consider all-to-all coupling in this case. This small change results in the emergence of a new synchronization phase, termed cluster synchronization as shown in Figs. 5(b,e). As the name suggests, there exist two clusters of synchronized CTCs with different frequencies. Further increasing the coupling strength to $\Gamma/\kappa = 1.25$ results in complete synchronization and these two clusters oscillate at the same frequency as shown in Figs. 5(c,f). These findings demonstrate that different choices of initial states can result in different regimes of synchronization.

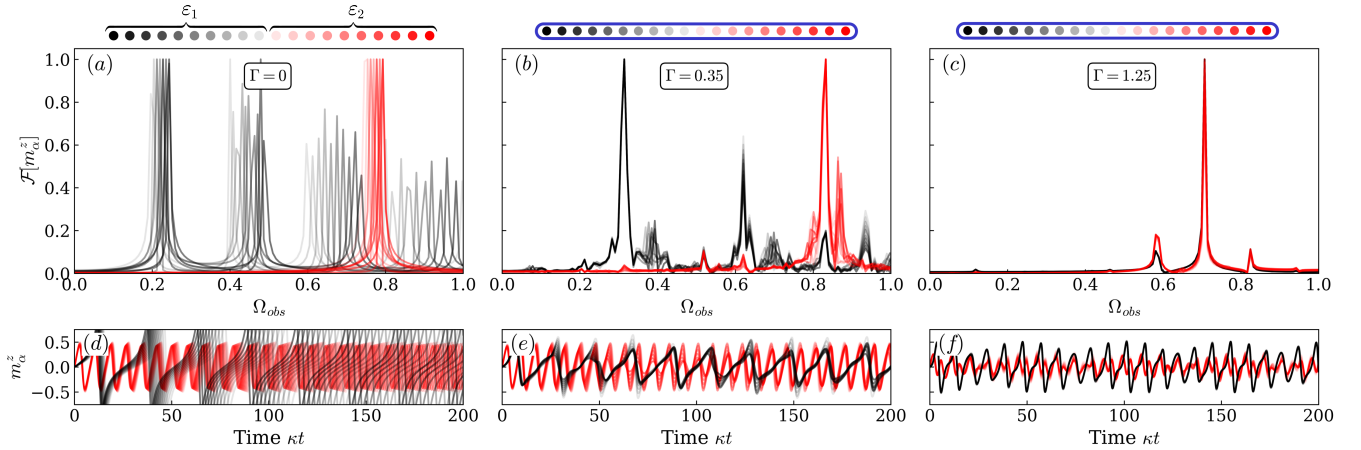


FIG. 5. Here we consider $n = 20$ CTCs having the same $\Omega_\alpha/\kappa = 0.9$ which are initialized with different m subspaces. Subfigure (a,d) represents uncoupled time crystals. For finite coupling strength $\Gamma/\kappa = 0.35$, there are two clusters of synchronized CTCs with different frequencies as shown in (b,e). At a coupling strength $\Gamma/\kappa = 1.25$, all the CTCs get synchronized as shown in (c,f).